NANO · MICRO small
www.small-journal.com

Self-Formation of a Ru/ZnO Multifunctional Bilayer for the Next-Generation Interconnect Technology via Area-Selective Atomic Layer Deposition

Yuki Mori, Taehoon Cheon, Yohei Kotsugi, Youn-Hye Kim, Yejin Park, Mohd Zahid Ansari, Debananda Mohapatra, Yujin Jang, Jong-Seong Bae, Woobin Kwon, Gahui Kim, Young-Bae Park, Han-Bo-Ram Lee, Wooseok Song, and Soo-Hyun Kim**

This study suggests a Ru/ZnO bilayer grown using area-selective atomic layer deposition (AS-ALD) as a multifunctional layer for advanced Cu metallization. As a diffusion barrier and glue layer, ZnO is selectively grown on SiO_2, excluding Cu, where Ru, as a liner and seed layer, is grown on both surfaces. Dodecanethiol (DDT) is used as an inhibitor for the AS-ALD of ZnO using diethylzinc and H_2O at 120 °C. H_2 plasma treatment removes the DDT adsorbed on Cu, forming inhibitor-free surfaces. The ALD-Ru film is then successfully deposited at 220 °C using tricarbonyl(trimethylenemethane) ruthenium and O_2. The Cu/bilayer/Si structural and electrical properties are investigated to determine the diffusion barrier performance of the bilayer film. Copper silicide is not formed without the conductivity degradation of the Cu/bilayer/Si structure, even after annealing at 700 °C. The effect of ZnO on the Ru/SiO_2 structure interfacial adhesion energy is investigated using a double-cantilever-beam test and is found to increase with ZnO between Ru and SiO_2. Consequently, the Ru/ZnO bilayer can be a multifunctional layer for advanced Cu interconnects. Additionally, the formation of a bottomless barrier by eliminating ZnO on the via bottom, or Cu, is expected to decrease the via resistance for the ever-shrinking Cu lines.

1. Introduction

The semiconductor industry and modern electronic devices require a stable metal interconnect and efficient diffusion barrier to minimize detrimental interactions. The selection and implementation of multifunctional diffusion barriers are essential and challenging to maintain the tradeoff. As the miniaturization of semiconductor devices progresses, device fabrication has faced many challenges.[1–3] The main challenge for the continued downscaling of integrated circuits is the increase in the resistance of the Cu interconnects due to a decrease in volume.[4] Furthermore, Cu interconnects require a highly resistive TaN diffusion barrier and Ta liner layer to prevent Cu diffusion into the dielectrics and improve the adhesion between Cu and the dielectrics.[5–8] As the size decreases, these layers occupy a large part of the interconnect cross-sectional area,

Y. Mori, Y. Kotsugi
Chemical Materials Development Department
TANAKA Precious Metals
22, Wadai, Tsukuba, Ibaraki 300–4247, Japan

Y. Mori, D. Mohapatra, S.-H. Kim
Graduate School of Semiconductor Materials and Devices Engineering
Ulsan National Institute of Science and Technology
50 UNIST-gil, Ulju-gun, Ulsan 44919, Republic of Korea
E-mail: soohyunsq@unist.ac.kr

T. Cheon, Y.-H. Kim, Y. Park, M. Z. Ansari
School of Materials Science and Engineering
Yeungnam University
280 Daehak-Ro, Gyeongsan, Gyeongsangbuk-do 38541, Republic of Korea

The ORCID identification number(s) for the author(s) of this article can be found under https://doi.org/10.1002/smll.202300290.

DOI: 10.1002/smll.202300290

Y. Jang, J.-S. Bae
Busan Center
Korea Basic Science Institute
30, Gwahaksandan 1-ro 60beon-gil, Gangseo-gu, Busan 46742, Republic of Korea

W. Kwon, G. Kim, Y.-B. Park
School of Materials Science and Engineering
Andong National University
Andong-si, Gyeongsangbuk-do 36729, Republic of Korea

H.-B.-R. Lee
Department of Materials Science and Engineering
Incheon National University
Incheon 22012, Republic of Korea

W. Song
Thin Film Materials Research Center
Korea Research Institute of Chemical Technology
Daejeon 34114, Republic of Korea
E-mail: wssong@krict.re.kr

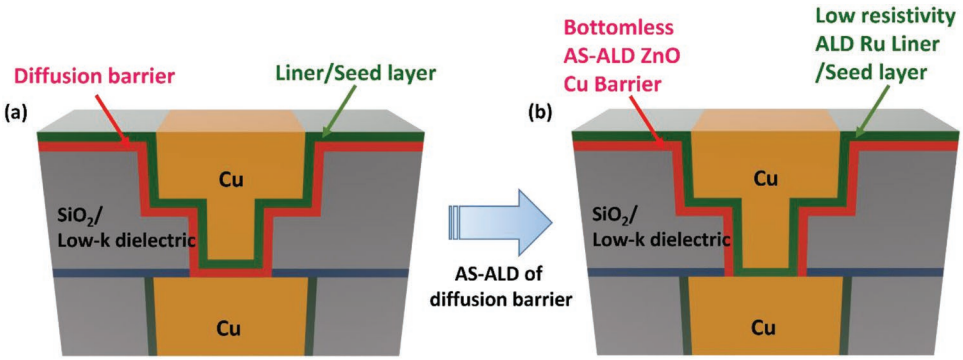

Figure 1. a) Schematic illustration of a typical via structure. b) Schematic illustration of a via structure consisting of a Ru/ZnO multifunctional bilayer using AS-ALD. The step coverage of diffusion barrier and liner/seed layer of (a) could be somewhat worse if the sputter-based deposition technology is used.

and the Cu area decreases further. This causes an increase in the resistance because of the decreasing dimensions of the Cu and the high resistivity of the barrier and liner materials compared to Cu. Accordingly, new interconnect materials, such as Ru, Co, Ir, Rh, and others, that have a lower resistivity at small dimensions and do not require barrier materials have been suggested and studied.[4] However, Cu is still expected to be the main conductor material because new interconnect materials are expected to be used for the narrowest structures, such as M0 and M1.[9] Therefore, eliminating or reducing the liner and/or barrier layers significantly reduces the interconnect resistance.[10]

Vias in the metallization structure are short vertical conductors connecting two levels of Cu interconnect lines (**Figure 1**a).[11] Vias also need a liner layer similar to that at the trench. The diffusion barrier at the bottom of the via only separates the two Cu regions and is not necessary;[12] however, because of the damascene integration scheme of Cu interconnects, it is redundantly located at the bottom of the via. Because the electrons that move vertically through the via must pass through the highly resistive diffusion barrier layer, the via resistance increases. As such, eliminating the diffusion barrier at the bottom of the via and implementing a Cu surface with only its growth on the sidewall of the via and trench is required for ever-shrinking semiconductor devices. This bottomless barrier can reduce the total barrier film thickness without reducing the barrier film thickness of the sidewalls. The diffusion barrier on the via bottom accounts for most of the high via resistance. Therefore, the interconnect resistance can be reduced by eliminating the diffusion barrier at the bottom of the via. To achieve a bottomless barrier, it is necessary to selectively deposit a diffusion barrier on only the dielectric and not on the metallic Cu surface.

Area-selective atomic layer deposition (AS-ALD) is a promising approach that provides a bottomless barrier. Because ALD is a film deposition method that utilizes a chemical reaction on the surface, it is possible to control the growth and non-growth surfaces by modifying the state of the surface.[13–15] The most common AS-ALD method uses inhibitors that passivate the surface. When inhibitors are adsorbed on the surface, they inhibit the adsorption of the precursor on the surface and cause nucleation delay during film growth. Self-assembled monolayers (SAMs) are among the most commonly used inhibitors. SAMs selectively adsorb only on a specific surface because of the head group and surface reaction. Additionally, the surface properties can be controlled by the functional groups of the SAM. Typically, transition metal nitrides, such as TaN, are used as the diffusion barrier for Cu metallization because of their ability to prevent metal diffusion and high stability at high temperatures.[16] The successful growth of transition metal nitrides using AS-ALD has been reported.[17–19] Lionti et al. reported the AS-ALD of TaN using (3-(12-(tricosa-11,13-diynoyloxy)dodecanamido)propyl)phosphonic acid as an inhibitor.[19] The inhibitor was selectively adsorbed onto W to form SAMs, which were polymerized using UV exposure or heat treatment because of the diyne moiety of the inhibitor. The polymerized SAMs exhibited high thermal stability, and a TaN film of up to 3.8 nm was deposited on SiN or SiCOH without TaN deposition on Cu or W during the TaN ALD process.[19] However, TaN requires a high deposition temperature above ≈300 °C, and common inhibitors, such as alkanethiols, are decomposed at these temperatures.[20] Therefore, TaN might not be suitable for AS-ALD using inhibitors. Merkx et al. reported the selective deposition of TiN on SiO_2 and Al_2O_3 and not on Co and Ru using aniline as an inhibitor.[21] TiN can also be used as a diffusion barrier for Cu interconnects; however, the deposition process of TiN is plasma-enhanced ALD (PE-ALD) using Ar-H_2 plasma as a reactant. Because the inhibitor adsorbed on the non-growth surface was removed due to the high reactivity of the radical species, it was necessary to supply the inhibitor every ALD cycle. This may cause a decrease in the growth per cycle (GPC) on the growth surface and the contamination of the film with impurities.[1] Additionally, a surface recombination of radical species causes the difficulty of the conformal deposition on very narrow-sized 3D structures like vias.[22] Due to the above concerns, a non-plasma process can be a better option for the film formation of the bottomless barrier.

Thermally grown AS-ALD-ZnO as a bottomless Cu diffusion barrier and as a glue layer for dielectric substrates is demonstrated for the first time in this study. ZnO was selected because ALD can deposit it at temperatures as low as 120 °C, a temperature at most of the inhibitors are thermally stable. Many studies have reported using AS-ALD for the successful growth of ZnO between SiO_2 and Cu substrates,[23–26] between a SiO_2 substrate and other dielectrics (Al_2O_3, HfO_2, TiO_2, and Ta_2O_5),[27] and

between a Si substrate and an Au substrate.[28] Additionally, the diffusion of Cu into ZnO requires heat treatment at high temperatures (> 1000 °C).[29] In a previous report by López-Salazar et al., the diffusion coefficient of Cu in ZnO was reported to be ≈2×10^{-12} cm^2 s^{-1} even at 1000 °C.[30] The value is slightly higher than in conventional TaN barriers (≈1×10^{-14} cm^2 s^{-1}) but significantly lower than in Si (≈1×10^{-4} cm^2 s^{-1}).[31,32] Although ZnO diffusion barriers have not been reported so far, ZnO thin films are expected to function as diffusion barriers for Cu interconnects. Furthermore, ZnO reacts with SiO_2 to form Zn_2SiO_4 at the interface.[33,34] Zn_2SiO_4 improves the interfacial adhesion energy between ZnO and SiO_2.[35,36] Wang et al. reported that the Zn doping of Ru films improved the interfacial adhesion energy through the diffusion of Zn and the formation of Zn_2SiO_4 at the interface between Ru and SiO_2.[37,38] RuZn alloy films were deposited by co-sputtering; however, it was challenging to selectively deposit them on via sidewalls. Furthermore, in this study, Ru thin films were grown using ALD on ZnO and Cu surfaces as a conformal and highly conductive metal liner/seed layer for electroplated (EP) Cu metal lines, forming a ZnO/Ru multifunctional bilayer on the dielectric surface and a single Ru layer without a ZnO barrier layer on the Cu surface. The interfacial adhesion energy and diffusion barrier performance of the Ru/ZnO bilayer were evaluated for their application in advanced Cu metallization (Figure 1b).

2. Results and Discussion

2.1. Exposure of Dodecanethiol (DDT) on Substrates Prior to ZnO ALD

The change in the surface conditions of the Cu and SiO_2 substrates after DDT exposure at 120 °C was analyzed using water contact angle (WCA) measurements (**Figure 2**a). The WCA on the Cu substrate increased with an increased exposure time and saturated at ≈107° after 15 s. In contrast, the WCA on the SiO_2 substrate did not change up to 90 s. The increase in the WCA value only on Cu substrates indirectly indicated the selective adsorption of DDT on Cu, but not on the SiO_2 substrates. The thermal stability of DDT adsorbed on Cu was also analyzed using WCA measurements of the DDT-exposed Cu surfaces (Figure S1, Supporting Information). The WCA value did not change at 120 °C, even after 16 h, indicating that DDT had good thermal stability on the Cu surface at the ZnO deposition temperature. Previous studies reported the WCA values on Cu substrates after DDT exposure to be ≈106–111° and that they depend on the Cu surfaces' oxidation state.[23–25,39] A WCA value of ≈106° is obtained on DDT-exposed Cu substrates with unoxidized Cu surfaces, whereas the WCA values change to ≈110–111° on Cu_2O and 106–107° on CuO.[39] Pristine Cu substrates with native oxides were used in this study. Therefore, the WCA results indicated that DDT was adsorbed on the Cu substrates with CuO surfaces. DDT etches CuO surfaces to create Cu-thiolate multilayers instead of SAMs.[40] These substrates were analyzed using X-ray photoelectron spectroscopy (XPS) to determine the selective adsorption of DDT. Figure 2b shows high-resolution XPS spectra within the 158–170 eV range for the S 2p peak on DDT-exposed Cu and SiO_2 substrates.[41] On the Cu substrates, large thiol $2p_{3/2}$ and $2p_{1/2}$ peaks were observed at 162.1 and 163.1 eV, respectively. These peaks were assigned to the Cu-bound thiolate. However, no S XPS peak was observed for the SiO_2 substrates. The WCA and XPS results confirm that DDT was selectively adsorbed on Cu substrates but not on SiO_2 substrates. The peak at ≈168 eV has been reported to be derived from sulfone [$R(SO_2)R'$],[40] which is thought to have been generated by the air oxidation of thiol during the sample delivery process for XPS analysis.

2.2. ZnO ALD on DDT-Exposed Substrates

To evaluate the blocking ability of DDT to prevent ZnO deposition on Cu surfaces, ZnO ALD was conducted on both DDT-exposed Cu and SiO_2 surfaces at 120 °C using diethylzinc (DEZ) and H_2O as the precursor and reactant, respectively. The DEZ and H_2O pulsing times were 1 s each, which guaranteed the self-limited growth of ZnO (Figure S2, Supporting

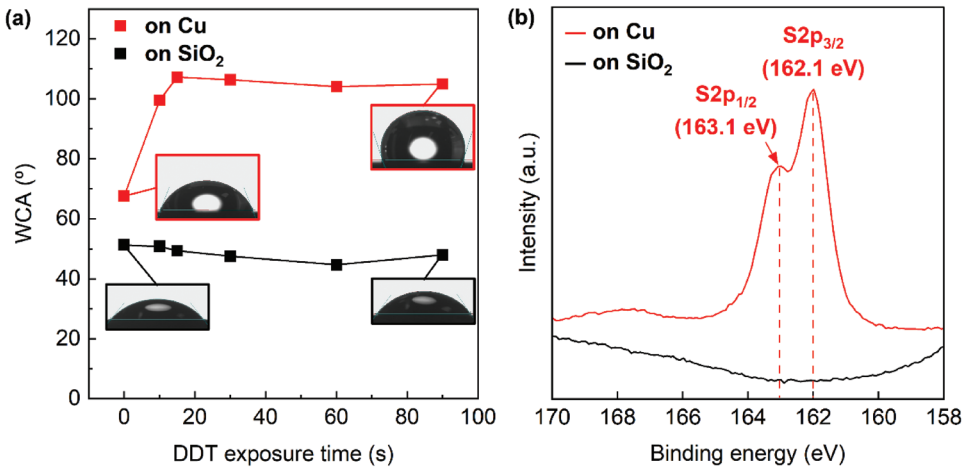

Figure 2. a) WCAs as a function of the DDT exposure time at 120 °C on Cu and SiO_2. Inset figures show contact angle images for droplets of the water on Cu and SiO_2 before and after DDT exposure. b) S 2p XPS spectra after DDT exposure on Cu and SiO_2.

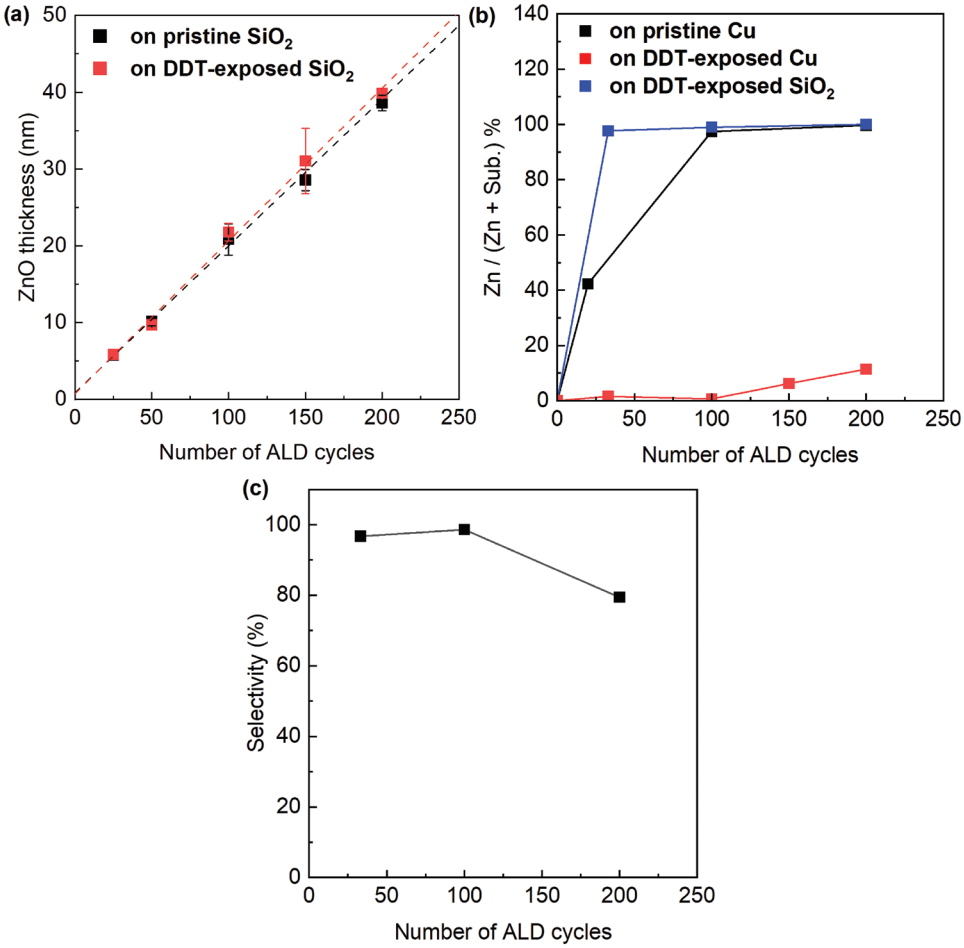

Figure 3. a) ZnO thickness on pristine and DDT-exposed SiO_2 substrates, b) atomic composition ratio of Zn on pristine Cu, DDT-exposed Cu, and DDT-exposed SiO_2 substrates, as determined from the XPS spectra, and c) selectivity as calculated by the atomic composition ratio of Zn on DDT-exposed Cu and SiO_2 substrates with an increasing number of ZnO ALD cycles.

Information). The thickness of ZnO and the atomic concentration of Zn on DDT-exposed substrates after different numbers of ZnO ALD cycles were analyzed using X-ray reflectometry (XRR), scanning electron microscopy (SEM), transmission electron microscopy (TEM), and XPS (**Figure 3**). The ZnO thickness measured on the DDT-exposed SiO_2 surface increased linearly, and there was almost no nucleation delay in the extrapolated thickness data. The GPC was ≈1.9 Å cycle^{-1}, which is similar to that of the pristine SiO_2 substrate (Figure 3a). The XPS spectra were evaluated to compare the change in the intensities of the Zn peaks on both pristine Cu and DDT-exposed Cu as a function of the number of ALD cycles (Figure S3, Supporting Information). The Zn concentration is related to the amount of ZnO on the surface. The Zn concentration on the pristine Cu increased with the number of ALD cycles. In contrast, the Zn concentration on the DDT-exposed Cu remained < 1 at% for up to 150 ZnO ALD cycles (Figure S4, Supporting Information). This indicates that DDT exposure effectively prevents ZnO deposition on Cu. Selectivity was calculated using Equation (1):[39,42]

$$S = \frac{R_{gs} - R_{ns}}{R_{gs} + R_{ns}} \quad (1)$$

where R_{gs} represents the atomic composition ratio of Zn on the DDT-exposed SiO_2 growth surface (gs), defined as Zn/(Zn+Si), and R_{ns} represents the atomic composition ratio of Zn on the DDT-exposed Cu non-growth surface (ns), defined as Zn/(Zn+Cu) (Figure 3b). Figure 3c shows the selectivity calculated using the atomic composition ratio of Zn on DDT-exposed Cu and SiO_2 as a function of the number of ALD cycles. The selectivity remained above 90% even after 100 cycles (≈20 nm), and the selectivity decreased with an increasing number of ALD cycles, with a value of ≈80% at 200 cycles. This is similar to the value reported in a previous study of AS-ALD ZnO on SiO_2 and Cu substrates using DDT.[23] The authors of the study compared the selectivities of Cu substrates with different surface oxidation states. Multilayer DDT was formed on the CuO surface, which was formed by the UV ozone cleaning of the Cu substrate. In contrast, monolayer DDT was formed on the Cu surface without surface oxides. The selectivity using multilayer DDT was approximately seven times more effective than that using monolayer DDT, and the selectivity was > 90% after at least 100 ZnO ALD cycles. The results show that high selectivity can be achieved using Cu substrates with a surface native oxide. X-ray diffraction (XRD) and cross-sectional TEM (XTEM) analyses

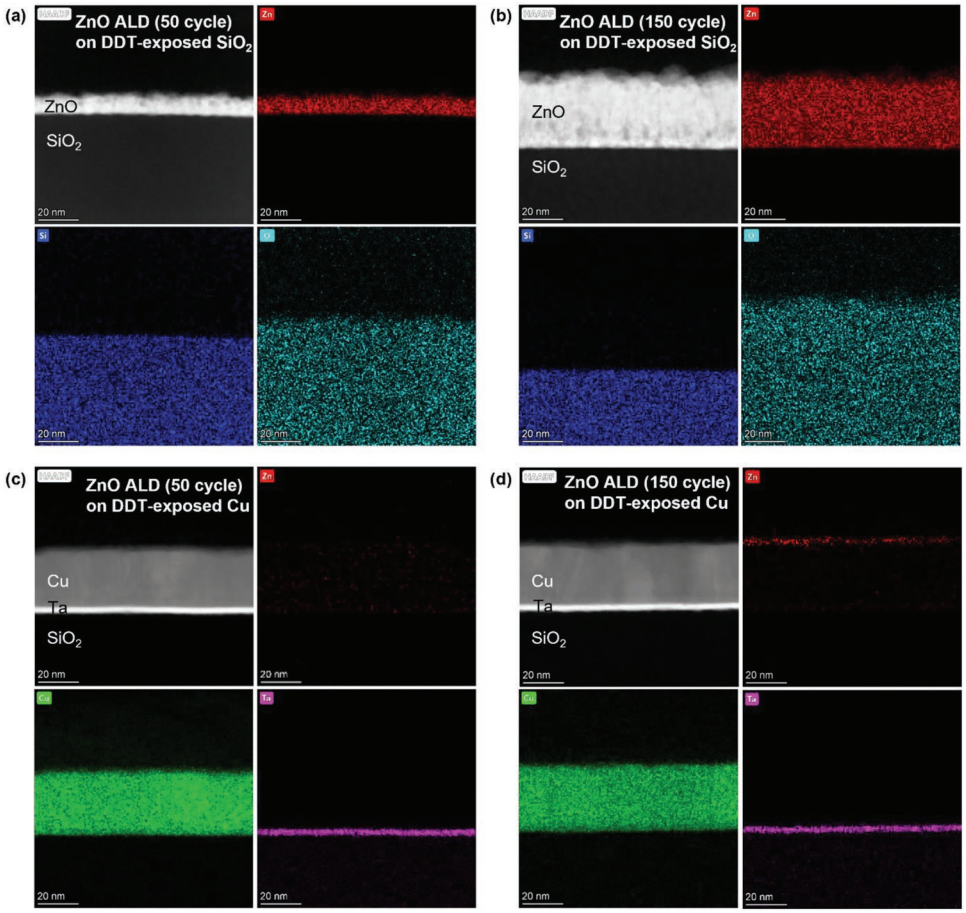

Figure 4. STEM-HAADF images and EDS mapping of a) ZnO-ALD (50 cycles) on DDT-exposed SiO_2, b) ZnO-ALD (150 cycles) on DDT exposed SiO_2, c) ZnO-ALD (50 cycles) on DDT-exposed Cu, and d) ZnO-ALD (150 cycles) on DDT-exposed Cu.

were performed further to analyze the selective ALD-ZnO films (Figure S5, Supporting Information). Figure S5a, Supporting Information shows the XRD results of the ALD-ZnO films after 150 cycles (≈30 nm) deposited on the DDT-exposed SiO_2 and Cu substrates. The selective growth of ZnO on the substrates can be clearly observed in the XRD results between 30° and 40° of 2 theta. ZnO peaks were observed on DDT-exposed SiO_2 but not on DDT-exposed Cu. Figure S5b–d, Supporting Information shows the XTEM results of the ALD-ZnO films deposited on DDT-exposed SiO_2 with 50 and 150 cycles and those deposited on the DDT-exposed Cu substrate with 150 cycles. ≈10 and 38 nm ALD-ZnO films were observed on DDT-exposed SiO_2 after 50 and 150 cycles, respectively. These results confirm that the thin thickness of the ZnO film on the SiO_2 substrate exposed to DDT increased with an increasing number of ALD cycles, whereas an ALD-ZnO film was hardly deposited on the Cu substrate exposed to DDT. The scanning TEM (STEM) high-angle annular dark field (HAADF) images and energy-dispersive X-ray spectroscopy (EDS) mapping results can clearly confirm these results in **Figure 4**. Figure 4a,b shows that ALD-ZnO grew well on the SiO_2 substrate exposed to DDT, consistent with the XTEM results. However, ALD-ZnO did not grow on the Cu substrate exposed to DDT (Figure 4c), and only a few nm of ALD-ZnO film deposited even after 150 cycles (Figure 4d). The thickness of ALD-ZnO film after 150 cycles deposited on DDT-exposed Cu was analyzed using XRR measurements. The thickness of ZnO was ≈2 nm. The result shows that ALD-ZnO was deposited on DDT-exposed Cu after 150 cycles, but the thickness is extremely thin compared to ALD-ZnO on DDT-exposed SiO_2. These results further support the selective deposition of ZnO on DDT-exposed SiO_2 but not on Cu.

2.3. H_2 Plasma Treatment for DDT Removal

To prevent potential contamination of the surface, DDT was removed before the deposition of Ru. Several methods for removing SAMs have been reported, such as acid treatment, UV irradiation, oxidation by O_3, thermal desorption, and plasma treatment.[43–47] Reagents in wet processes, such as acid treatment, cause contamination. Oxidation processes, such as UV irradiation and oxidation by O_3, might oxidize the Cu surfaces, whereas thermal desorption causes incomplete decomposition and contamination of impurities on the substrate. In contrast, plasma treatment enables SAMs to decompose into volatile fragments, which can be removed by purging. Raiber et al. reported the removal of hexadecanethiol SAMs

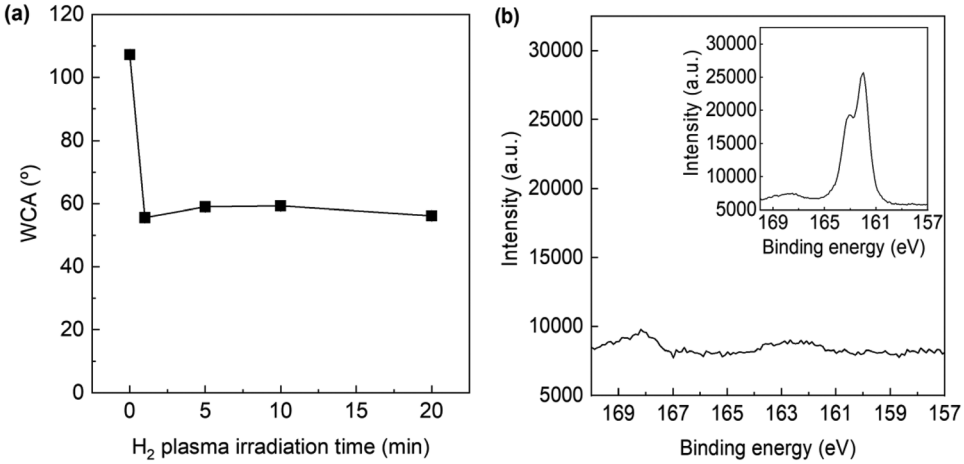

Figure 5. Confirmation of the removal of DDT from the Cu surface as characterized using a) WCA measurements and b) XPS after the H_2 plasma treatment at 150 °C for 5 min. Inset figure shows the XPS analysis result before the H_2 plasma treatment.

on Au surfaces using plasma treatment.[47] They used H_2 and O_2 plasmas to remove SAMs and compared the efficiencies of the different plasmas. They confirmed that both plasmas could remove SAMs, but O_2 plasma caused the oxidized Au surface to be contaminated with oxidized S species. This study determined the ability of H_2 plasma treatment to remove SAMs on Cu. The change in the surface conditions after a H_2 plasma treatment at 150 °C was analyzed using WCA measurements and XPS (**Figure 5**). The WCA was decreased by the H_2 plasma and then saturated after 1 min (Figure 5a), indicating the formation of bare Cu surfaces with a low WCA owing to their hydrophilicity due to the removal of DDT. Additionally, the elemental compositions of the Cu surfaces after a H_2 plasma treatment for 5 min were analyzed using XPS (Figure 5b). The peak intensity of S on the Cu substrates decreased, indicating that the H_2 plasma treatment removed the DDT on Cu. It is known that alkanethiols adsorbed on metal surfaces can be removed using reductive desorption.[48–51] In this study, it is thought that the reduction by H_2 plasma caused DDT desorption from the Cu surfaces. DDT on Cu was also removed by thermal treatment at high temperatures (Figure S6, Supporting Information). However, the efficiency of DDT removal was significantly lower than that of the H_2 plasma treatment.

2.4. Ru-ALD on DDT-Removed Substrates

As explained above, ZnO was selectively deposited at 120 °C on SiO_2 but not on Cu by the selective adsorption of DDT on the Cu surface. A H_2 plasma treatment successfully removed DDT at 150 °C for 5 min, and the inhibitor-free Cu surface was regenerated. Subsequently, Ru-ALD was conducted on ZnO and DDT-removed Cu surfaces at 220 °C by using tricarbonyl(trimethylenemethane)ruthenium [Ru(TMM)$(CO)_3$] and O_2 as a precursor and reactant, respectively, to grow a highly conductive liner/seed layer of Cu. XRR measured the thickness of Ru after 50 cycles, and the thickness of Ru after 100, 150, and 200 cycles was measured by SEM (**Figure 6**a). The thickness of Ru measured on both ZnO, and DDT-removed Cu surfaces increased linearly, and a very short nucleation delay

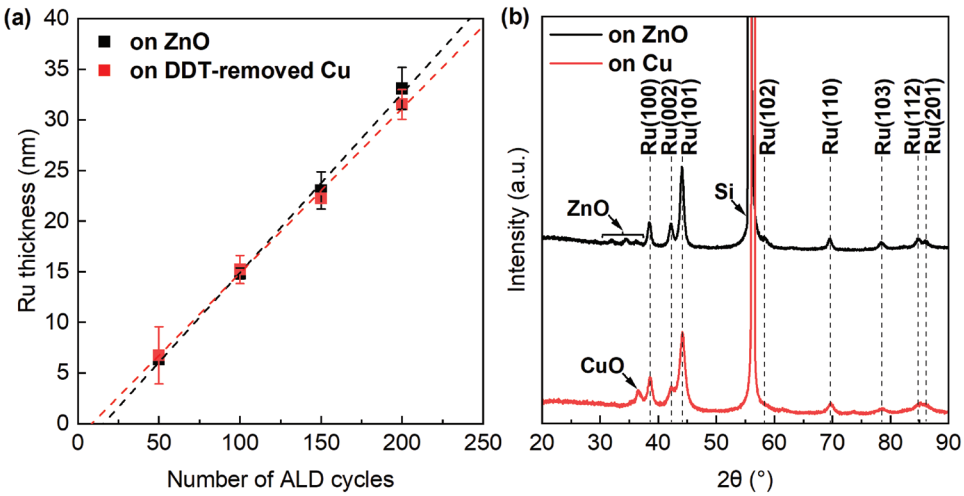

Figure 6. a) Thickness of the ALD-Ru films deposited on ZnO and DDT-removed Cu surfaces as a function of the number of ALD cycles and b) XRD patterns of ALD-Ru films deposited on ALD-ZnO and DDT-removed Cu surfaces.

(≈9 cycles) was observed in the extrapolated thickness data. The GPC was ≈1.7 Å cycle^{-1} on both substrates, which is similar to that reported previously for [Ru(TMM)(CO)$_3$] O$_2$-ALD on SiO$_2$ substrates.[52] Figure 6b shows the XRD results of the ALD-Ru films deposited on the ZnO and DDT-removed Cu surfaces. Similar HCP-Ru XRD spectra were observed on both substrates. The resistivities of the ALD-Ru films grown on both substrates were as low as ≈22 $\mu\Omega$·cm, which is significantly lower than that of typical liner/seed layer materials for Cu interconnects, such as ALD-Ta (150–180 $\mu\Omega$·cm) and ALD-Co (50–285 $\mu\Omega$·cm).[53–56] The conformity of the ALD-grown Ru liner/seed layer and the ZnO diffusion barrier is important for their use in vias. Previous studies have reported that Ru bilayer films have diffusion barrier properties against Cu.[57–60] However, their conformities are poor because they are deposited by sputtering. However, in this study, the application of ALD processes using DEZ and H$_2$O for ZnO[61,62] and [Ru(TMM)(CO)$_3$] and O$_2$ for Ru[52] guaranteed excellent step coverage on high-aspect-ratio 3D structures. Additionally, the formation of the closed layer is also important for the high diffusion barrier performance. The XTEM was performed to observe the morphology of the Ru/ZnO bilayer (Figure S7, Supporting Information). The XTEM image shows the morphology of the film consists of densely packed continuous Ru and ZnO layers. This result suggests that this Ru/ZnO bilayer is suitable as a diffusion barrier.

2.5. Performance of the Ru/ZnO Multifunctional Layer

The Ru/ZnO bilayer investigated in this study was proposed as a multifunctional layer for advanced Cu metallization, where ZnO functions as a diffusion barrier and glue layer and the highly conductive Ru film acts as a liner for Cu[63,64] and a seed layer for Cu EP.[65–67] This study evaluated the diffusion barrier performance of the ALD-Ru/ALD-ZnO bilayer against Cu, 1 or 2 nm ALD-ZnO, and 4 nm ALD-Ru that were deposited on Si substrates followed by Cu deposition by sputtering on a Ru/ZnO bilayer. The multilayer structure of the Cu/bilayer of the Ru/ZnO/Si wafer was annealed under high-vacuum conditions (< 10^{-6} Torr) at 500–750 °C. To compare the diffusion barrier performance of the Ru/ZnO bilayer, annealing was performed on the structure with an ALD-Ru (5 nm) single layer between Cu and Si as a reference. Copper films with a thickness of 60 nm were deposited on all samples by sputtering. **Figure 7**a–c shows the XRD patterns of the films annealed at 500–750 °C for 10 min. The XRD results of the Cu (60 nm)/Ru (5 nm)/Si films (Figure 7a) show that intense Cu peaks were still observed after annealing at 500 °C, and their peak intensities were increased, as compared to the sample before annealing, indicating that Cu diffusion into Si did not occur, and the crystallinity of the Cu film improved. However, after annealing at 550 °C, the intensities of the Cu peaks drastically decreased, and most of the Cu peaks disappeared. Instead, new peaks related to Cu silicides and Cu$_3$Si and Cu$_{15}$Si$_4$ were observed.[58] This indicates that Ru failed as a diffusion barrier due to the diffusion of Cu into Si at this temperature. In the case of the Cu (60 nm)/Ru (4 nm)/ZnO (1 nm)/Si films (Figure 7b), strong Cu peaks were still observed after annealing at 550 °C, and peaks from Cu$_3$Si and Cu$_{15}$Si$_4$ were observed after annealing at 650 °C. By increasing the thickness of ZnO to 2 nm, the structure of Cu (60 nm)/Ru (4 nm)/ZnO (2 nm)/Si became stable up to 700 °C (Figure 7c). Peaks from Cu silicides were observed after annealing at 750 °C. These results confirm that the diffusion of Cu was drastically hindered by inserting a very thin ALD-ZnO layer between Ru and Si.

Sheet resistance measurements were performed to further understand the diffusion barrier performance of the Ru/ZnO bilayer through its electrical conduction properties. Figure 7d shows the sheet resistances of the Cu (60 nm)/ALD-Ru (5 nm)/Si, Cu (60 nm)/ALD-Ru (4 nm)/ALD-ZnO (1 nm)/Si, and Cu (60 nm)/ALD-Ru (4 nm)/ALD-ZnO (2 nm)/Si samples as a function of the post-annealing temperature. The sheet resistance of Cu (60 nm)/ALD-Ru (5 nm)/Si initially decreased after annealing at 500 °C, which was due to the improvement in the crystallinity of the Cu film and defect annihilation in the Cu film during annealing, because most of the current in this structure is carried by a highly conductive and relatively thick Cu film instead of Ru. This phenomenon was reflected in the XRD results of the sample after annealing at 500 °C (Figure 7a), where the intensities of the Cu peaks were significantly increased and their full width at half maximum was narrowed. The sheet resistance of the Cu (60 nm)/ALD-Ru (5 nm)/Si structure began to increase after annealing at 550 °C and increased drastically after annealing at 600 °C, indicating that the diffusion barrier failed at that temperature. In fact, various Cu silicides with significantly higher resistivity than Cu were observed after annealing at 550 °C (Figure 7a). Both the formation of Cu silicides and the consumption of highly conductive Cu owing to the diffusion of Cu through the Ru single layer contributed to the increase in the sheet resistance after annealing at temperatures > 550 °C. In contrast, the sheet resistance of Cu (60 nm)/ALD-Ru (4 nm)/ALD-ZnO (1 nm)/Si did not change until the samples were annealed at 600 °C. When the temperature was increased to 650 °C, where the formation of Cu silicides was observed (Figure 7b), the sheet resistance increased. Upon increasing the thickness of ZnO to 2 nm, the sheet resistance of Cu (60 nm)/ALD-Ru (4 nm)/ALD-ZnO (2 nm) was stable up to 700 °C and started to increase after annealing at 750 °C with the formation of Cu silicides (Figure 7c). These results suggest that by adding a very thin (1 nm) ZnO layer to Ru, its barrier performance against Cu was significantly enhanced (improvement up to 100 °C), which was further enhanced by increasing the thickness of the ZnO layer. Table S1, Supporting Information shows a summary of diffusion barrier materials deposited by ALD. In previous reports, a bilayer and alloys containing Ru, nitrides, and oxides have been reported as barrier materials. Compared to these materials, the Ru/ZnO bilayer shows low resistivity and high failure temperature with relatively thin film thickness. It indicates that Ru/ZnO bilayer is a promising candidate of bottomless diffusion barrier for Cu interconnects.

The measured interfacial adhesion energy of the Cu/Ru (5 nm)/SiO$_2$ structure using a double cantilever beam (DCB) test was 0.87 ± 0.13 J m^{-2} and it was delaminated between Ru and SiO$_2$. However, the interfacial adhesion energy of the Cu/Ru (4 nm)/ZnO (2 nm)/SiO$_2$ structure, as measured using a DCB test, was 2.21 ± 0.39 J m^{-2} and it was delaminated between ZnO and SiO$_2$. This increase in the interfacial adhesion energy

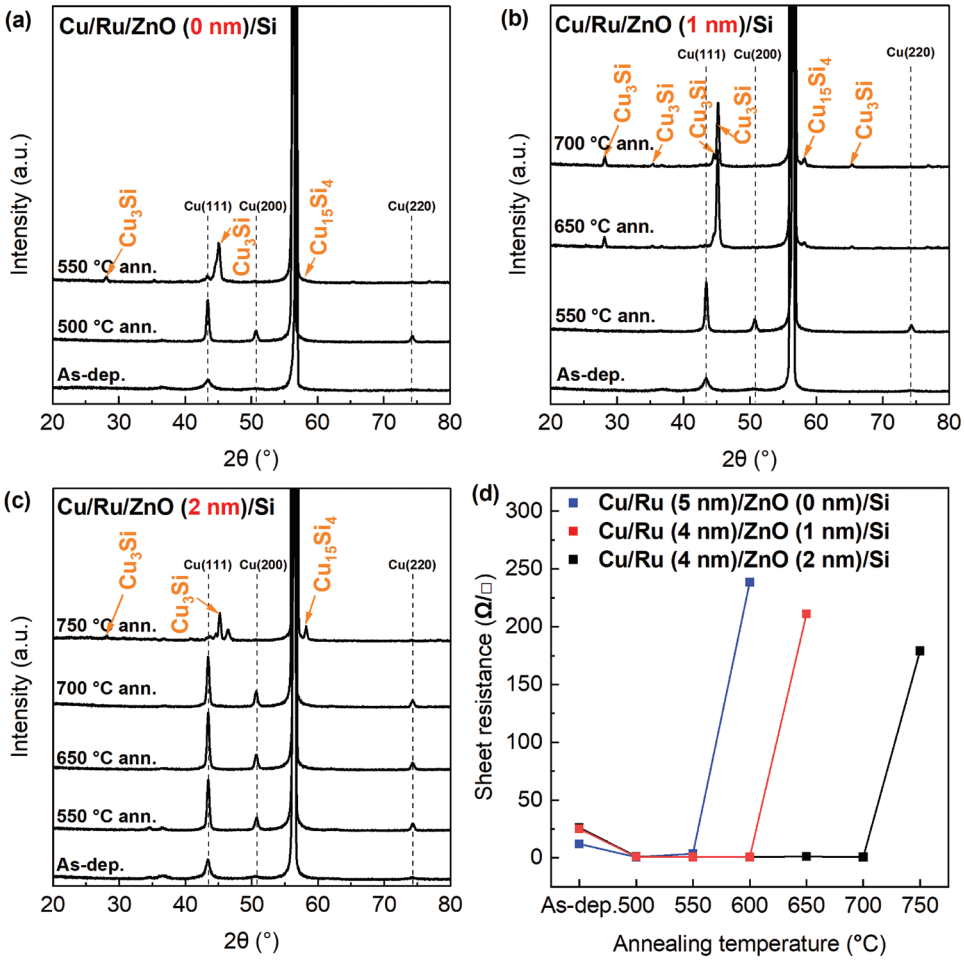

Figure 7. XRD results of a) the Cu (60 nm)/ALD-Ru (5 nm)/ALD-ZnO (0 nm)/Si, b) Cu (60 nm)/ALD-Ru (4 nm)/ALD-ZnO (1 nm)/Si, c) and Cu (60 nm)/ALD-Ru (4 nm)/ALD-ZnO (2 nm)/Si structures after annealing at different temperatures. d) Sheet resistance of the Cu (60 nm)/ALD-Ru (5 nm)/ALD-ZnO (0 nm)/Si, Cu (60 nm)/ALD-Ru (4 nm)/ALD-ZnO (1 nm)/Si, and Cu (60 nm)/ALD-Ru (4 nm)/ALD-ZnO (2 nm)/Si structures after annealing.

is due to the ZnO diffusion barrier between Ru and SiO_2. Previous studies reported that the measured interfacial adhesion energy of the Cu/Ru/SiO_2 structure using a four-point bending (4-PB) test was ≈3 J m^{-2}.[68–70] Additionally, previous studies have reported that the minimum limit criterion of the interfacial adhesion energy is 5 J m^{-2}, which is defined as the criterion for the back-end of the line process to prevent delamination during chemical mechanical polishing.[71] However, this criterion can only be applied in the case of the 4-PB test. The phase angles (ratio of modes) of the DCB and 4-PB tests were 0° and 43°, respectively. The interfacial crack during the DCB test was almost tensile; therefore, the phase angle was ≈0°. However, the 4-PB test is a mixed mode in which both tensile and shear stresses are applied to the sample, but the shear stress is more dominant; therefore, the phase angle is larger than that of the DCB test.[72–76] This can be explained by the increased interfacial adhesion energy according to phase angle due to the effect of the higher roughness-related shielding and plastic energy dissipation of the 4-PB test than that of the DCB test.[72] Furthermore, the interfacial adhesion energy measured using the 4-PB test was approximately three to five times higher than that measured by the DCB test.[72] Therefore, the interfacial adhesion energy of each sample structure measured using the 4-PB test is expected to be higher than the value measured using the DCB test.

3. Conclusions

In this study, ZnO thin films were selectively deposited only on SiO_2 surfaces and not on Cu surfaces using DDT as an inhibitor during the ZnO-ALD process at 120 °C. Through the selective adsorption of DDT on the Cu surface, the high selectivity of ZnO-ALD was maintained for up to 100 ALD cycles. After the AS-ALD of ZnO, DDT adsorbed on the Cu surface could be easily removed using a H_2 plasma treatment at temperatures as low as 150 °C. Ruthenium thin films as liner/seed layers for Cu metallization were grown on both ALD-ZnO and DDT-removed Cu surfaces by Ru-ALD at 220 °C using [Ru(TMM)$(CO)_3$] and O_2. The XRD and sheet resistance results showed that the diffusion barrier performance of Ru (4 nm)/ZnO (1, 2 nm) against Cu was drastically improved, as compared to

that against an Ru (5 nm) single layer. The DCB test results indicated that the Ru (4 nm)/ZnO (2 nm) bilayer exhibited excellent interfacial adhesion energy (≈2.21 J m^{-2}), as compared to that of a Ru (5 nm) single layer (≈0.87 J m^{-2}) between the Cu and SiO_2 dielectric. Thus, the results suggest that the Ru/ZnO bilayer is a promising candidate for a multifunctional layer as a diffusion barrier, liner, and seed layer for advanced Cu metallization. Moreover, it can be further expected that a low via resistance can be achieved using the AS-ALD-ZnO diffusion barrier, which is only deposited on the SiO_2 dielectric surface and not on the Cu surface, demonstrating the successful application of AS-ALD in semiconductor device processing.

4. Experimental Section

Exposure of DDT on Substrates: Inhibitor exposure on Cu and SiO_2 substrates prior to ZnO ALD was performed in a traveling-wave-type ALD reactor (Lucida-D100, NCD Technology), where ZnO and Ru were used. DDT (> 98%, Sigma-Aldrich) and N_2 were used as the inhibitor and purging gas, respectively. DDT was stored in a stainless-steel canister, which was maintained at 85 °C. The DDT adsorption process was optimized as a function of the substrate temperature and DDT exposure time. The temperature of the substrates was maintained in the range of 100–260 °C. The idle time after the DDT pulse was set at 80 s for sufficient exposure to the substrate by closing the pumping line, and the purging time was 120 s.

ZnO-ALD on DDT-Exposed Substrates: ZnO-ALD was performed to evaluate the blocking properties of the DDT inhibitor. The blocking test was performed in a thermal ALD system with a base pressure of 0.15 Torr, and the substrate temperature was maintained at 120 °C. For the ZnO-ALD, DEZ (EG Chem Co., Ltd.) and H_2O were used as the precursor and reactant, respectively. Both DEZ and H_2O were stored in stainless-steel canisters, which were maintained at 10 °C using a cooling system to control their vapor pressure. The gas flow rate of the purging N_2 was 100 standard cubic centimeters per minute (sccm). One cycle of ZnO-ALD was composed of a 1 s DEZ pulse, 10 s N_2 purge, 1 s H_2O pulse, and 30 s N_2 purge. The GPC of the ZnO-ALD on the DDT-exposed SiO_2 substrates was ≈1.9 Å $cycle^{-1}$.

H_2 Plasma Etching for DDT Removal: H_2 plasma etching using a shower-head type plasma-enhanced ALD reactor (Lucida-M100, NCD Technology) was performed to remove the DDT on the substrates. The plasma source was a capacitively coupled plasma type with a direct plasma operation. The H_2 gas flow rate was 30 sccm, and the radio frequency power was 100 W. The chamber pressure during plasma etching was maintained at ≈0.4 Torr.

Ruthenium-ALD on DDT-Removed Substrates: Ruthenium-ALD was performed using the same thermal ALD reactor with [Ru(TMM)$(CO)_3$] (TANAKA Precious Metals, Japan) and O_2 as the precursor and reactant, respectively.[52] [Ru(TMM)$(CO)_3$] was stored in a stainless-steel canister, which was maintained at 10 °C using a cooling system. The Ru precursor was pulsed and carried into the chamber by N_2 gas at a flow rate of 50 sccm. The gas flow rates of reactant O_2 and purging N_2 were 50 and 100 sccm, respectively. The deposition temperature was 220 °C. One cycle of Ru ALD was composed of a 10 s [Ru(TMM)$(CO)_3$] pulse, 10 s N_2 purge, 10 s O_2 pulse, and 10 s N_2 purge. Ruthenium films were deposited on ZnO (4 nm)/SiO_2 and DDT-removed Cu substrates. The GPC of the Ru ALD was ≈1.7 Å $cycle^{-1}$.

Characterization of the Film Properties: WCA measurements were performed using an optical contact angle measuring and contour analysis system (OCA 20, Dataphysics Instruments) to confirm the change in the surface hydrophobicity caused by the adsorption of DDT. The thicknesses of the ALD-grown films were determined using XRR (PANalytical X'-Pert MRD, Cu Kα radiation at 1.5 kW) and field-emission SEM (S-4800, Hitachi). Phase identification was performed using grazing incidence angle XRD (PANalytical X'-Pert MRD) analysis with Cu Kα radiation at a wavelength (λ) of 1.5406 Å and a grazing-incidence angle of $\omega = 3°$. The sheet resistances of the films were measured using a four-point probe station. The film compositions were analyzed using XPS (ESCALAB 250, monochromatic Al Kα source, VG Scientific, KBSI Busan Center) using XTEM (Tecnai F20 equipped with 200 kV accelerating voltage) and a focused ion-beam technique for sample preparation. EDS analysis was performed using the same TEM equipment.

Diffusion Barrier Test: The diffusion barrier performance of the Ru/ZnO bilayer between Cu and Si was evaluated. For the evaluation, 60 nm-thick Cu films were sputter-deposited onto a Ru/ZnO bilayer on Si wafers. The thickness of ZnO was varied from 1 to 2 nm to evaluate the effect of the thickness of the ZnO bottomless barrier on the diffusion barrier performance against Cu. These Cu/bilayer (Ru/ZnO)/Si samples were then annealed under high vacuum (< 10^{-6} Torr) for 10 min at temperatures ranging from 500 to 750 °C at intervals of 50 °C. For comparison, a structure without the ZnO barrier, Cu/Ru/Si, was prepared and post-annealed. The barrier performance after annealing was evaluated using sheet resistance measurements and XRD.

Interfacial Adhesion Energy Measurement: A sample was fabricated, as shown in Figure S8, Supporting Information, to investigate the effect of the ZnO diffusion barrier between Ru and SiO_2 on the interfacial adhesion energy. Additionally, a DCB test was conducted to evaluate the interfacial adhesion energy. To form a sandwich structure, thin films were deposited on a 625 µm-thick, 6-inch Si wafer. Figure S8a,b, Supporting Information shows schematics of the Cu (60 nm)/Ru (5 nm) and Cu (60 nm)/Ru (4 nm)/ZnO (2 nm) multilayer thin film sandwich structures between Si wafers for the DCB test. To prepare the sandwich structure, a 100 nm thick SiO_2 thin film was deposited on a Si wafer using a thermal oxidation process. Then, a 5 nm-thick Ru film was deposited on SiO_2 with 35 ALD cycles, and a 60 nm-thick Cu layer was deposited on the Ru film by sputtering. Additionally, a 2 nm-thick ZnO layer was deposited on SiO_2 with 10 ALD cycles, and a 4 nm-thick Ru film was deposited on ZnO with 30 ALD cycles. Subsequently, a 60 nm-thick Cu layer was deposited on the Ru film by sputtering. To prepare the DCB test sample, the deposited Si wafer and a dummy Si wafer (with thermally grown SiO_2) were cut into 10×40 mm^2 rectangular pieces. An epoxy adhesive (EPO-TEK 353ND, Epoxy Technology Inc.) was applied to the surface of the dummy Si wafer, which was attached to create a sandwich structure. Subsequently, the epoxy adhesive was cured at 120 °C for 2 h. The epoxy adhesive was not applied in the pre-crack; therefore, the sample was not bonded in this area. Aluminum loading taps were attached to the upper and lower sides of the DCB test sample using a commercial adhesive (DP-420, 3 M), as shown in Figure S8c, Supporting Information. The commercial adhesive was then cured at 80 °C for 30 min. The fracture mechanics of the DCB test samples were tested using a micromechanical test system (Mini Microload Tester; R&B Inc., Korea). The sample was loaded and unloaded at a consistent displacement rate of 0.03 mm min^{-1}. The applied load was continuously measured as a function of the displacement, as shown in Figure S9, Supporting Information.[77,78] The sample was initially loaded elastically. However, crack propagation occurred along the weak interface between the thin film and Si wafer once the strain-energy release rate exceeded the interfacial adhesion energy between the thin film and Si wafer. At this critical point, the gradient of the load–displacement curve started to decrease, considering the changes in the sample compliance with the propagation of the crack. The beam was unloaded during the continuous propagation of the crack by several millimeters. Subsequently, several additional multiple instances of loading, crack propagation, and unloading cycles were applied to the beam. The crack length (a) and interfacial adhesion energy (G_c) were calculated using Equations (2) and (3):[77,79–81]

$$a = \left(\frac{CE'bh^3}{8}\right)^{\frac{1}{3}} - 0.64h \tag{2}$$

$$G_c = \frac{12P_c^2a^2}{E'b^2h^3}\left(1 + 0.64\frac{h}{a}\right)^2 \tag{3}$$

where C, E', b, h, and P_c are the sample compliance, plane strain modulus of the beam (Si wafer:169 GPa), sample width (10 mm), half of the beam thickness (625 µm), and critical load where the gradient of the load–displacement curve started to decrease, respectively.

Supporting Information

Supporting Information is available from the Wiley Online Library or from the author.

Acknowledgements

Y.M. and T.C. contributed equally to this work. This study was supported by the National Research Foundation of Korea (NRF) grants funded by the Korean Government (Ministry of Science and ICT) (2021M3H4A3A02099209, 2021R1A2C1007601, 2022R1A2C1092453).

Conflict of Interest

The authors declare no conflict of interest.

Data Availability Statement

The data that support the findings of this study are available from the corresponding author upon reasonable request.

Keywords

area-selective atomic layer deposition, Cu metallization, diffusion barriers, Ru liner, ZnO

Received: January 10, 2023
Revised: March 23, 2023
Published online: May 1, 2023

[1] J. Yarbrough, A. B. Shearer, S. F. Bent, *J. Vac. Sci. Technol., A* **2021**, *39*, 021002.
[2] H.-B.-R. Lee, *Chem. Mater.* **2019**, *31*, 1471.
[3] R. Chen, Y.-C. Li, J.-M. Cai, K. Cao, H.-B.-R. Lee, *Int. J. Extreme Manuf.* **2020**, *2*, 022002.
[4] D. Gall, *J. Appl. Phys.* **2020**, *127*, 050901.
[5] L. Y. Yang, D. H. Zhang, C. Y. Li, P. D. Foo, *Thin Solid Films* **2004**, *462*, 176.
[6] J. Bryner, D. M. Profunser, J. Vollmann, E. Mueller, J. Dual, *Ultrasonics* **2006**, *44*, e1269.
[7] N. Fréty, F. Bernard, J. Nazon, J. Sarradin, J. C. Tedenac, *J. Phase Equilib. Diffus.* **2006**, *27*, 590.
[8] Q. Xie, X.-P. Qu, J.-J. Tan, Y.-L. Jiang, M. Zhou, T. Chen, G.-P. Ru, *Appl. Surf. Sci.* **2006**, *253*, 1666.
[9] M. Moore, *International Roadmap for Devices and Systems 2021*, IEEE, Piscataway, NJ **2021**.
[10] C.-L. Lo, B. A. Helfrecht, Y. He, D. M. Guzman, N. Onofrio, S. Zhang, D. Weinstein, A. Strachan, Z. Chen, *J. Appl. Phys.* **2020**, *128*, 080903.
[11] N. A. Lanzillo, K. Motoyama, H. Huang, R. R. Robison, T. Spooner, *Appl. Phys. Lett.* **2020**, *116*, 164103.
[12] M. J. M. Merkx, A. J. M. Mackus, Area-Selective ALD of Diffusion Barriers for via Optimization – There is Plenty of Room at the Bottom, https://www.atomiclimits.com/2022/04/18/area-selective-ald-of-diffusion-barriers-for-via-optimization-there-is-plenty-of-room-at-the-bottom/, (accessed: April 2022).
[13] G. N. Parsons, R. D. Clark, *Chem. Mater.* **2020**, *32*, 4920.
[14] A. J. M. Mackus, M. J. M. Merkx, W. M. M. Kessels, *Chem. Mater.* **2019**, *31*, 2.
[15] N. P. Dasgupta, H.-B.-R. Lee, S. F. Bent, P. S. Weiss, *Chem. Mater.* **2016**, *28*, 1943.
[16] Z. Li, Y. Tian, C. Teng, H. Cao, *Materials* **2020**, *13*, 5049.
[17] H. Kawasaki, M. Iwashita, H. Warashina, H. Nagai, K. Iwai, H. Komatsu, Y. Ozaki, G. Pattanaik, *2021 IEEE International Interconnect Technology Conference (IITC)*, IEEE, Piscataway, NJ **2021**, pp. 1–3.
[18] S. You, H. Ren, M. Naik, L. Chen, F. Chen, C. L. Cervantes, X. Xie, K. Kashefizadeh, *2021 IEEE International Interconnect Technology Conference (IITC)*, IEEE, Piscataway, NJ **2021**, pp. 1–3.
[19] K. Lionti, N. Arellano, N. Lanzillo, S. Nguyen, P. S. Bhosale, H. Bui, T. Topuria, R. J. Wojtecki, *Chem. Mater.* **2022**, *34*, 2919.
[20] Y.-H. Lai, C.-T. Yeh, S.-H. Cheng, P. Liao, W.-H. Hung, *J. Phys. Chem. B* **2002**, *106*, 5438.
[21] M. J. M. Merkx, S. Vlaanderen, T. Faraz, M. A. Verheijen, W. M. M. Kessels, A. J. M. Mackus, *Chem. Mater.* **2020**, *32*, 7788.
[22] H. C. M. Knoops, T. Faraz, K. Arts, W. M. M. Kessels, *J. Vac. Sci. Technol., A* **2019**, *37*, 030902.
[23] T.-L. Liu, K. L. Nardi, N. Draeger, D. M. Hausmann, S. F. Bent, *ACS Appl. Mater. Interfaces* **2020**, *12*, 42226.
[24] F. S. M. Hashemi, B. R. Birchansky, S. F. Bent, *ACS Appl. Mater. Interfaces* **2016**, *8*, 33264.
[25] F. S. M. Hashemi, S. F. Bent, *Adv. Mater. Interfaces* **2016**, *3*, 1600464.
[26] F. S. M. Hashemi, C. Prasittichai, S. F. Bent, *J. Phys. Chem. C* **2014**, *118*, 10957.
[27] T.-L. Liu, S. F. Bent, *Chem. Mater.* **2021**, *33*, 513.
[28] W. Dong, K. Zhang, Y. Zhang, T. Wei, Y. Sun, X. Chen, N. Dai, *Sci. Rep.* **2014**, *4*, 4458.
[29] F. Herklotz, E. V. Lavrov, J. Weber, *Phys. B* **2009**, *404*, 4807.
[30] P. López-Salazar, G. Juárez-Díaz, J. Martínez-Juárez, J. A. Luna-López, R. Peña Sierra, Y. Koudriavtsev, C. Palomino-Jiménez, A. P. Rodríguez-Victoria, *Crystals* **2019**, *9*, 131.
[31] C. Lee, Y.-L. Kuo, *JOM* **2007**, *59*, 44.
[32] A. A. Istratov, C. Flink, H. Hieslmair, E. R. Weber, *Phys. Rev. Lett.* **1998**, *81*, 1243.
[33] H. He, Y. Wang, Y. Zou, *J. Phys. D: Appl. Phys.* **2003**, *36*, 2972.
[34] C. Li, Z. Liang, H. Xiao, Y. Wu, Y. Liu, *Mater. Lett.* **2010**, *64*, 1972.
[35] A. Teraoka, M. Watanabe, Y. Nabetani, E. Kondoh, *Jpn. J. Appl. Phys.* **2013**, *52*, 05FB04.
[36] M. Watanabe, A. Teraoka, E. Kondoh, *Jpn. J. Appl. Phys.* **2014**, *53*, 05GA02.
[37] W. Peng, X.-P. Qu, Y. Dordi, *2020 IEEE International Interconnect Technology Conference (IITC)*, IEEE, Piscataway, NJ **2020**, pp. 115–117.
[38] P. Wang, X.-P. Qu, Y. Dordi, A. Joi, *J. Mater. Sci.: Mater. Electron.* **2022**, *33*, 6318.
[39] T.-L. Liu, S. F. Bent, *Adv. Mater. Interfaces* **2022**, *9*, 2200587.
[40] D. S. Bergsman, T.-L. Liu, R. G. Closser, K. L. Nardi, N. Draeger, D. M. Hausmann, S. F. Bent, *Chem. Mater.* **2018**, *30*, 5694.
[41] C. Vericat, M. E. Vela, G. Corthey, E. Pensa, E. Cortés, M. H. Fonticelli, F. Ibañez, G. E. Benitez, P. Carro, R. C. Salvarezza, *RSC Adv.* **2014**, *4*, 27730.
[42] D. Bobb-Semple, K. L. Nardi, N. Draeger, D. M. Hausmann, S. F. Bent, *Chem. Mater.* **2019**, *31*, 1635.
[43] J. M. Campiña, A. Martins, F. Silva, *Electrochim. Acta* **2008**, *53*, 7681.
[44] H.-S. Choi, Y. Kang, H. Lee, C. Lee, *Curr. Appl. Phys.* **2007**, *7*, 522.
[45] C. G. Worley, R. W. Linton, *J. Vac. Sci. Technol., A* **1995**, *13*, 2281.
[46] E. Delamarche, B. Michel, H. Kang, C. Gerber, *Langmuir* **1994**, *10*, 4103.

[47] K. Raiber, A. Terfort, C. Benndorf, N. Krings, H.-H. Strehblow, *Surf. Sci.* **2005**, *595*, 56.
[48] M. Yuan, S. Zhan, X. Zhou, Y. Liu, L. Feng, Y. Lin, Z. Zhang, J. Hu, *Langmuir* **2008**, *24*, 8707.
[49] J. A. Williams, C. B. Gorman, *J. Phys. Chem. C* **2007**, *111*, 12804.
[50] M. M. Walczak, D. D. Popenoe, R. S. Deinhammer, B. D. Lamp, C. Chung, M. D. Porter, *Langmuir* **1991**, *7*, 2687.
[51] X. Cai, S. Baldelli, *J. Phys. Chem. C* **2011**, *115*, 19178.
[52] Y. Kotsugi, S.-M. Han, Y.-H. Kim, T. Cheon, D. K. Nandi, R. Ramesh, N.-K. Yu, K. Son, T. Tsugawa, S. Ohtake, R. Harada, Y.-B. Park, B. Shong, S.-H. Kim, *Chem. Mater.* **2021**, *33*, 5639.
[53] H. Kim, C. Cabral, C. Lavoie, S. M. Rossnagel, *J. Vac. Sci. Technol., B: Microelectron. Nanometer Struct.–Process., Meas., Phenom.* **2002**, *20*, 1321.
[54] H.-B.-R. Lee, H. Kim, *ECS Trans.* **2008**, *16*, 219.
[55] H.-B.-R. Lee, W.-H. Kim, J. W. Lee, J.-M. Kim, K. Heo, I. C. Hwang, Y. Park, S. Hong, H. Kim, *J. Electrochem. Soc.* **2010**, *157*, D10.
[56] J.-H. Park, D.-Y. Moon, D.-S. Han, Y.-J. Kang, S.-R. Shin, H.-T. Jeon, J.-W. Park, *Surf. Coat. Technol.* **2014**, *259*, 98.
[57] X.-P. Qu, J.-J. Tan, M. Zhou, T. Chen, Q. Xie, G.-P. Ru, B.-Z. Li, *Appl. Phys. Lett.* **2006**, *88*, 151912.
[58] W. Sari, T.-K. Eom, C.-W. Jeon, H. Sohn, S.-H. Kim, *Electrochem. Solid-State Lett.* **2009**, *12*, H248.
[59] C.-X. Yang, S.-J. Ding, D. W. Zhang, P.-F. Wang, X.-P. Qu, R. Liu, *Electrochem. Solid-State Lett.* **2011**, *14*, H84.
[60] T.-K. Eom, W. Sari, T. Cheon, S.-H. Kim, W. K. Kim, *Thin Solid Films* **2012**, *521*, 73.
[61] J. W. Elam, D. Routkevitch, P. P. Mardilovich, S. M. George, *Chem. Mater.* **2003**, *15*, 3507.
[62] M. Ladanov, P. Algarin-Amaris, G. Matthews, M. Ram, S. Thomas, A. Kumar, J. Wang, *Nanotechnology* **2013**, *24*, 375301.
[63] H. Kim, T. Koseki, T. Ohba, T. Ohta, Y. Kojima, H. Sato, Y. Shimogaki, *J. Electrochem. Soc.* **2005**, *152*, G594.
[64] O.-K. Kwon, S.-H. Kwon, H.-S. Park, S.-W. Kang, *J. Electrochem. Soc.* **2004**, *151*, C753.
[65] O. Chyan, T. N. Arunagiri, T. Ponnuswamy, *J. Electrochem. Soc.* **2003**, *150*, C347.
[66] R. Chan, T. N. Arunagiri, Y. Zhang, O. Chyan, R. M. Wallace, M. J. Kim, T. Q. Hurd, *Electrochem. Solid-State Lett.* **2004**, *7*, G154.
[67] T. N. Arugagiri, Y. Zhang, O. Chyan, M. El-Bouanani, M. J. Kim, K. H. Chen, C. T. Wu, L. C. Chen, *Appl. Phys. Lett.* **2005**, *86*, 083104.
[68] H. Li, D. B. Farmer, R. G. Gordon, Y. Lin, J. Vlassak, *J. Electrochem. Soc.* **2007**, *154*, D642.
[69] T. E. Hong, T. Cheon, S.-H. Kim, J.-K. Kim, Y.-B. Park, O. J. Kwon, M. J. Kim, J. J. Kim, *J. Alloys Compd.* **2013**, *580*, 72.
[70] L. G. Wen, P. Roussel, O. V. Pedreira, B. Briggs, B. Groven, S. Dutta, M. I. Popovici, N. Heylen, I. Ciofi, K. Vanstreels, F. W. Østerberg, O. Hansen, D. H. Petersen, K. Opsomer, C. Detavernie, C. J. Wilson, S. V. Elshocht, K. Croes, J. Bömmels, Z. Tokei, C. Adelmann, *ACS Appl. Mater. Interfaces* **2016**, *8*, 26119.
[71] E. Andideh, T. Scherban, B. Sun, J. Blaine, C. Block, B. Jin, *Proceedings of the IEEE 2001 International Interconnect Technology Conference*, IEEE, Piscataway, NJ **2001**, pp. 257–259.
[72] M. Lane, *Annu. Rev. Mater. Res.* **2003**, *33*, 29.
[73] W. Broughton, *Testing the Mechanical, Thermal and Chemical Properties of Adhesives for Marine Environments, in: Adhesives in Marine Engineering*, Woodhead Publishing Ltd., Sawston **2012**.
[74] W. Yao, Y. Xu, C. Yu, K. Xia, *Eng. Fract. Mech.* **2017**, *176*, 161.
[75] M. R. Ayatollahi, A. R. Torabi, *Int. J. Solids Struct.* **2010**, *47*, 454.
[76] J. W. Hutchinson, Z. Suo, *Adv. Appl. Mech.* **1991**, *29*, 63.
[77] T.-S. Kim, N. Tsuji, N. Kemeling, K. Matsushita, D. Chumakov, H. Geisler, E. Zschech, R. H. Dauskardt, *J. Appl. Phys.* **2008**, *103*, 064108.
[78] T. Yoon, W. C. Shin, T. Y. Kim, J. H. Mun, T.-S. Kim, B. J. Cho, *Nano Lett.* **2012**, *12*, 1448.
[79] I. Lee, S. Kim, J. Yun, I. Park, T.-S. Kim, *Nanotechnology* **2012**, *23*, 485704.
[80] R. J. Hohlfelder, D. A. Maidenberg, R. H. Dauskardt, Y. Wei, J. W. Hutchinson, *J. Mater. Res.* **2001**, *16*, 243.
[81] M. F. Kanninen, *Int. J. Fract.* **1973**, *9*, 83.